Stem Cell Reviews and Reports (2022) 18:2088–2103
https://doi.org/10.1007/s12015-022-10418-9

# Human Umbilical Cord-Derived Mesenchymal Stem Cells Ameliorate Skin Aging of Nude Mice Through Autophagy-Mediated Anti-Senescent Mechanism

**Ting Li[1,2] · Li Zhou[3] · Mengqiang Fan[3] · Zuxiang Chen[3] · Li Yan[4] · Haishan Lu[5] · Ming Jia[6] · Huiling Wu[1,2] · Letian Shan[3,4]**

Accepted: 22 June 2022 / Published online: 21 July 2022


## Abstract

Skin aging is a currently irreversible process, affected by increased oxidative stress, activated cellular senescence, and lacked regeneration of the dermal layer. Mesenchymal stem cells (MSCs), such as human umbilical cord-derived MSCs (hucMSCs), have pro-regeneration and anti-aging potencies. To explore whether hucMSCs can be used to treat skin aging, this study employed skin-aging model of nude mice to conduct in vivo assays, including biochemical analysis of superoxide dismutase (SOD) and malondialdehyde (MDA), gross observation, histopathological observation, and immunohistochemical analysis. To clarify how hucMSCs work on skin aging, this study employed skin-aging model of human dermal fibroblasts (HDFs) to conduct in vitro assays by applying conditional medium of hucMSCs (CMM), including wound healing assay, senescence staining, flow cytometric oxidative detection, real time PCR, and western blot analysis. The in vivo data demonstrated that hucMSCs dose-dependently removed wrinkles, smoothed skin texture, and increased dermal thickness and collagen production of aged skin by reversing SOD and MDA levels and up-regulating Col-1 and VEGF expressions, indicating anti-oxidative and pro-regenerative effects against skin aging. The in vitro data revealed that hucMSCs significantly reversed the senescence of HDFs by promoting cell migration, inhibiting ROS production, and restoring the overexpressions of oxidative and senescent markers through paracrine mode of action, and the paracrine mechanism was mediated by the inhibition of autophagy. This study provided novel knowledge regarding the anti-aging efficacy and paracrine mechanism of hucMSCs on skin, making hucMSCs-based therapy a promising regime for skin aging treatment.

**Keywords** Skin aging · Senescence · Human umbilical cord-derived mesenchymal stem cells · Conditional medium · Autophagy

## Introduction

Skin is the largest organ of human body, exhibiting intuitive consequence of aging. Skin aging is affected by both extrinsic and intrinsic factors, such as ultraviolet radiation, air pollution, mitochondria respiration, and excessive accumulation of glycogen, which may result in oxidative stress outcomes [1–3]. Oxidative stress is the core mechanism mediating skin aging, induced by the accumulation of reactive oxygen species, thus leading to cellular senescence [4]. In the dermal layer of skin, reactive oxygen species (ROS)

Ting Li and Li Zhou contributed equally to this work.

✉ Huiling Wu
zywhl@zju.edu.cn

✉ Letian Shan
letian.shan@zcmu.edu.cn

[1] The First Affiliated Hospital, College of Medicine, Zhejiang University, Hangzhou, China

[2] Department of Plastic and Aesthetic Center, The First Affiliated Hospital of Zhejiang University, Hangzhou, China

[3] The First Affiliated Hospital, Zhejiang Chinese Medical University, Hangzhou, China

[4] Cell Resource Bank and Integrated Cell Preparation Center of Xiaoshan District, Hangzhou Regional Cell Preparation Center (Shangyu Biotechnology Co., Ltd), Hangzhou, China

[5] Department of Dermatology, PLA 903 Hospital, Hangzhou, China

[6] Affiliated Hangzhou First People's Hospital, Zhejiang University School of Medicine, Hangzhou, China

is mainly produced by the primary cell type, human dermal fibroblasts (HDFs) [3, 5]. Under the normal condition, HDFs produces macromolecules, such as proteoglycans, glycosaminoglycans, collagen, elastin, fibrin, and hyaluronic acid, to compose the extracellular matrix (ECM) and support the mechanical resistance and elasticity to skin [3, 5, 6]. With oxidative stress, HDFs may suffer senescence and produce not only ROS but also matrix-degrading metalloproteinases (MMPs) to degrade ECM [7, 8]. Skin elasticity is thereby decreased with phenotypes of dry, loose and rough, leading to deep and thick wrinkles [9, 10]. Recent studies have revealed that nuclear factor kappa B (NF-κB) is one of the master regulators of oxidative stress-induced senescence, promoting the transcription of MMPs and affecting ECM composition [7, 11, 12]. Besides, autophagy has been reported to regulate the skin homeostasis and critically participate in the aging process of skin [13]. Autophagy can be activated with senescence of fibroblasts or in response to oxidative stress, and the inhibition of autophagy-related protein 5 (ATG5) may delay the occurrence of senescence in skin [14–16]. Thus, the regime which suppresses NF-κB or autophagy may possess anti-aging potential against skin.

Antioxidants, such as resveratrol, tea polyphenols, vitamin C and vitamin E, are deemed to scavenge ROS, neutralize free radicals, and inhibit activity of MMPs and collagenases, thereby increasing skin elasticity and reversing thick skin wrinkles [9, 17–20]. However, those antioxidants have several disadvantages that restricted their clinical application in anti-aging treatment. For instance, resveratrol has low bioavailability due to its nature of rapid metabolism in human body, resulting in inadequate role at the acting sites [7, 21]. Moreover, effective and safe dose range of tea polyphenols is not yet determined, and vitamin C and E are potentially unstable due to the inherent instability and low penetrability of micronutrients to skin layers [19, 22]. Photoelectric technologies, such as lasers and light-based treatments, are also employed to treat skin aging by promoting fibroblast proliferation and collagen synthesis [23]. However, their efficacies are not sufficient to relieve the skin aging symptoms while their side effects are sometimes present in clinic [23, 24]. Accordingly, it is necessary and significant to develop new approaches with certain effectiveness and safety for skin aging treatment.

Mesenchymal stem cells (MSCs) are multipotent stromal cells possessing capabilities of multi-lineage differentiation potential, high proliferation and self-renewal, making them an ideal candidate of cell therapy for tissue regeneration [25]. MSCs were firstly identified from bone marrow and thereafter obtained from various tissues, such as umbilical cord, muscle and fat [26, 27]. Studies have reported that adipose- and bone marrow-derived MSCs exerted positive effects on skin and other tissues, but the ethical concerns regarding the invasive and painful obtainment procedure of these MSCs have limited their availability [28–32]. As a medical waste, umbilical cord is regarded as a better source of MSCs with little ethical constraints, owing to its non-invasiveness of obtainment and high accessibility [33]. Besides, human umbilical cord derived MSCs (hucMSCs) are seemingly "younger " than that from other resources because hucMSCs are isolated from neonatal tissue, which may be endowed with improved multipotency, enhanced stemness, superior clonogenicity, lesser immunogenicity, higher migrative and homing activities, and longer proliferative and better paracrine capacities [33–35]. Moreover, the immunomodulatory and angiogenic potencies of hucMSCs can be maintained after cryopreservation and subsequent thawing, whereas those potencies of adipose tissue-derived MSCs (ADSCs) and bone marrow–derived MSCs (BMSCs) would be impaired after cryopreservation [36, 37]. Hence, hucMSCs might be the most promising candidate of stem cells for autologous and allogeneic application. To date, hucMSCs has been widely studied for the treatments of knee osteoarthritis, perinatal brain injury, diabetic wound healing, exhibiting anti-inflammatory, pro-regenerative and anti-aging activities [38–40]. Nevertheless, little study has focused on the anti-aging efficacy of hucMSCs on skin aging.

To firstly determine the efficacy and explore the underlying mechanism of hucMSCs on skin aging, this study employed a classic skin-aging model of nude mice and a dermis-aging model of HDFs by using D-galactose (D-gal). D-gal-induced skin aging by inducing oxidative stress, ROS accumulation, and cell senescence, which has been routinely used to mimic intrinsic or natural skin aging [41]. This study may evidence hucMSCs-based therapy as a potentially promising strategy for anti-aging treatment.

## Materials and Methods

### Reagents and Materials

High D-Glucose Dulbecco's Modified Eagle Medium (DMEM) and phosphate buffered saline (PBS) was purchased from Gibco BRL (NY, USA). Fetal bovine serum (FBS) was purchased from CellMax (Beijing, China). Trypsin (0.25%) was purchased from Thermo Fisher Scientific (MA, USA). Enzyme-linked immunosorbent assay (ELISA) kits were bought from MultiSciences (Lianke) Biotech Co., Ltd (Hangzhou, China). Cell culture plates were purchased from Eppendorf (Hamburg, Germany). Radioimmunoprecipitation assay (RIPA) buffer and proteinase inhibitor cocktails were purchased from Bimake (TX, USA). TRIzol reagent and DNase I kit were obtained from TaKaRa Biotechnology Co. Ltd. (Dalian, China). All-in-One cDNA Synthesis SuperMix kit was purchased from Biotool (TX, USA). 2×SYBR Green qPCR Master Mix (low ROX)

kit was obtained from Bimake (TX, USA). β-actin (A3854, 1:10,000) was purchased from Sigma Aldrich (USA), p65 (8242S, 1:1000), phosphorylated p65 (p-p65) (Ser536) (3033S, 1:1000), p21 (2947S, 1:1000), p62 (5114 T, 1:1000) and LC3B (3968S, 1:1000) were purchased from Cell Signaling Technology Inc. (MA, USA). LaminB1 (66,095–1-lg, 1:1000) and HMGB1 (10,829–1-AP, 1:1000) were purchased from Proteintech Group Inc (Illinois, USA). p16 (5114 T, 1:1000) was purchased from Abcam Trading Co., Ltd (Cambridge, UK). Nitrocellulose membrane was bought from Sartorius Stedim Biotech (Göttingen, Germany). Western Lightning® Plus ECL was obtain from Perkin Elmer, Inc. (Waltham, MA, USA) and Biosharp (Beijing, China). Senescent cells histochemical staining kit were obtained from Beyotime Biotechnology (Shanghai, China). Detect reactive oxygen species H2DCFDA was purchased from AbMole (Shanghai, China). Chloroquine (NSC-187208, Aralen, CQ) and Rapamycin (AY-22989) were bought from Selleck.

## HucMSCs Isolation and Identification

The section of human umbilical cord (Wharton's jelly) was obtained from the first affiliated hospital of Zhejiang Chinese Medical University with the permission of donors and was freshly processed within 4 h. The umbilical cord was cut into pieces with $< 2$ $cm^3$ volume and washed with PBS (pH 7.4) for 3 times. After removal of epidermal tissue and vessel endothelium, samples were immersed in α-MEM containing 10% FBS at 37 °C and 5% CO2 for incubation. The culture medium was renewed every 2 or 3 days. The isolated cells were collected as hucMSCs and resuspended in α-MEM containing 10% FBS, with passage being carried out after confluence had occurred.

Identification of the hucMSCs phenotype was performed by flow cytometry. The cells were suspended in PBS at a density of $10^6$ cells/ml and incubated with CD34, CD45, CD73, CD90, CD105 and HLA-DR mouse antihuman antibodies, respectively. After incubation for 30 min at room temperature, each cell suspension was centrifuged at 2000 rpm for 5 min. The supernatant was removed and 100 µl PBS were added to resuspend the cell pellet for flow cytometry analysis (BD FACSVerse, NJ, USA).

## Animal Experiments

A total of 30 healthy SPF grade BALB/c nude male mice (6-week-old), weighing 18-22 g, were provided by Shanghai Slack Company, animal production license number (SCXK: 2017–0005 Shanghai, Zhejiang, China). The mice were raised by the Animal Experiment Research Center of Zhejiang Chinese Medical University. All mice were housed in the controlled room with constant temperature (22 ± 2 °C), humidity 50 ~ 60%, light and dark alternately every 12 h, and allowed ad libitum food and water. All mice were treated in strict accordance with the China legislation on the use and care of laboratory animals. All experiments on the mice were approved by the Medical Norms and Ethics Committee of Zhejiang Chinese Medical University.

The mice were randomly divided into five groups: normal control group, skin aging model group (Model), low dose of hucMSCs group (hucMSCs-L), medium dose of hucMSCs group (hucMSCs-M), and high dose of hucMSCs group (hucMSCs-H). The model group and all hucMSCs groups were treated with subcutaneous injection of D-gal dissolved in 0.9% normal saline to the back at a dose rate of 1500 mg/kg /day (BW/day). NC group was treated with 0.9% normal saline for comparison. After D-gal aging modeling for six weeks, mice in hucMSCs-L, hucMSCs-M, and hucMSCs-H groups were subcutaneously injected with 0.25 ml of hucMSCs resuspended in 1 ml PBS ($10^6$cells/ml, $10^5$cells/ml, $10^4$cells/ml, respectively). Meanwhile, NC group was subcutaneously injected with 0.25 ml of saline solution. The D-gal injection and saline solution sites are same as the cell's injection site. All treatments were weekly conducted for 2 weeks, and thereby all the mice were sacrificed and the pieces of skin from the back were taken for histological and biochemical examination. Prior to the experiments, after modeling and hucMSCs treatments, mice in different groups were photographed to record skin changes and score skin grades. Skin state was graded according to the appearances of skin textures and wrinkles (Table1).

## Skin Superoxide Dismutase (SOD) and Malondialdehyde (MDA) Analysis in Nude Mice

Skin tissue samples from the back of nude mice in different groups are weighed. Skin samples were cut and added physiological saline to produce the 10% homogenate, and then sonicated twice every 30 s at 4 °C. After sonication, the homogenate was centrifuged at 3,000 rpm for 10 min. An aliquot of the supernatant was used for further experiments. BCA protein determination kit was used to determine the protein content of aliquots. MDA and SOD kits were used to detect the content of SOD and MDA in the skin samples, according to each manufacturer's instructions.

## Histopathological Observation and Immunohistochemical Analysis

skin samples were fixed with 4% buffered Paraformaldehyde for 48 h at room temperature. Then the samples were embedded in paraffin and sectioned into 4 µm, followed by HE (hematoxylin and eosin) staining and Masson staining. The stained sections were pictured by a light microscope (Axio Scope A1, ZEISS, Germany) and statistically by Image J 1.47 software (Version

**Table 1** Skin grades of nude mice

| Grades | Skin state description |
|---|---|
| 0 | The primary line and the secondary line have the same depth, clearly visible and intersected. Wrinkles are thin and superficial |
| 1 | The secondary lines are flattened, and the number is reduced. A few wrinkles are shallowly coarse |
| 2 | The primary line becomes uneven, the secondary line becomes obviously flat or deformed, and the number of intersections is reduced. Some wrinkles are coarse |
| 3 | The texture is deteriorated, the primary lines are thick and deep, a large flat skin appears between the primary lines, and secondary lines are deformed and disappeared. Wrinkles are deeply coarse and wide |

1.6.0) (Media Cybernetics, Bethesda, MD, USA). Unstained replicates of the sections were incubated overnight at 4 °C with 1000 μl PBS-diluted (1:1000) primary antibodies against mice Col-1 and VEGF for immunohistochemical staining. After PBS wash, the sections were incubated with Horseradish peroxidase (HRP) conducted secondary antibodies for 1 h at room temperature, followed by 2-(4-amidinophenyl)-6-indolecarbamidine dihydrochloride (DAPI) staining Solution for 5 min. The skin sections were visualized under a light microscope (Axio Scope A1, ZEISS, Germany). The immunoreactivity of Col-1 and VEGF were semiquantified by Image J 1.47 software.

## Cell Culture and Modeling

HDFs were provided by Kunming Cell Bank of Chinese Academy of Sciences (KCB200537). HDFs were cultured with high-glucose DMEM supplemented with 10% FBS and maintained in 37 °C incubator with 5% $CO_2$ and 95% humidity. Senescent HDFs modeling was established by the treatment of D-gal at 20 g/l concentration for 48 h. HucMSCs were switched to high-glucose DMEM with 10% FBS and incubated for two days to generate the conditional medium of hucMSCs (CMM) for treatment.

## Analysis of Excretions of hucMSCs

Concentration of total protein in the CMM and free medium (DMEM) were measured by using BCA Protein concentration assay kit in accordance with the manufacturer′s instructions. The concentrations of hepatocyte growth factor (HGF), epidermal growth factor (EGF), fibroblast growth factor (FGF), and vascular endothelial growth factor (VEGF) in the CMM were measured by using the corresponding ELISA kits in accordance with the manufacturer′s instructions.

## Wound Healing Assay

HDFs in the logarithmic growth phase were seeded into 6-well plates ($1 \times 10^5$ cells/well), modeled with D-gal at 20 g/l for 48 h and artificially scratched to form wound area, followed by treatment of CMM. The cells were observed and imaged at 0 h, 24 h and 48 h using an inverted microscope (CarlZeiss, Göttingen, Germany). The scratched area was measured using by Image J 1.47 software. Each experiment was conducted in triplicate.

## Senescence-Associated-Beta-Galactosidase (SA-β-gal) Staining

HDFs were plated in 6-well plates ($1 \times 10^5$/well), modeled with D-gal at 20 g/l for 48 h and followed by CMM treatment for 48 h. The HDFs were thereby fixed with 4% paraformaldehyde and SA-β-Gal stained using senescent cells staining kit, according to each manufacturer's instructions. Three images per each well were collected, and the SA-β-Gal-stained cells were counted by Image J 1.47 software. Each experiment was conducted in triplicate.

**Table 2** Primer sequences used for qPCR analysis

| Gene | Forward primer | Reverse primer |
|---|---|---|
| *β-actin* | 5′-CCCGCGAGTACAACCTTCT-3′ | 5′-CGTCATCCATGGCGAACT-3′ |
| *MMP1* | 5′-GTGCAGACGCCAGAAGAATCT-3′ | 5′-TGTCACACGCTTTTGGGGTTT -3′ |
| *MMP3* | 5′- GAGGCATCCACACCCTAGGTT-3′ | 5′-TCAGAAATGGCTGCATCGATT-3′ |
| *P21* | 5′-GGCAGACCAGCATGACAGATT-3′ | 5′-GCGGATTAGGGCTTCCTCT-3′ |
| *P16* | 5′-CATGGTGCGCAGGTTCTTG-3′ | 5′-CGGGATGTGAACCACGAAA-3′ |
| *P65* | 5′-CCACGAGCTTGTAGGAAAGG-3′ | 5′-CTGGATGCGCTGACTGATAG-3′ |
| *SOD1* | 5′-ACTCTCAGGAGACCATTGCATCA-3′ | 5′-TCCTGTCTTTGTACTTTCTTCATTTCC-3′ |
| *IL-6* | 5′-GCCACTGCCTTCCCTACTTCA-3′ | 5′-GACAGTGCATCATCGCTGTTCA-3′ |
| *Col-1* | 5′-GAGGGCCAAGACGAAGACATC-3′ | 5′-CAGATCACGTCATCGCACAAC-3′ |

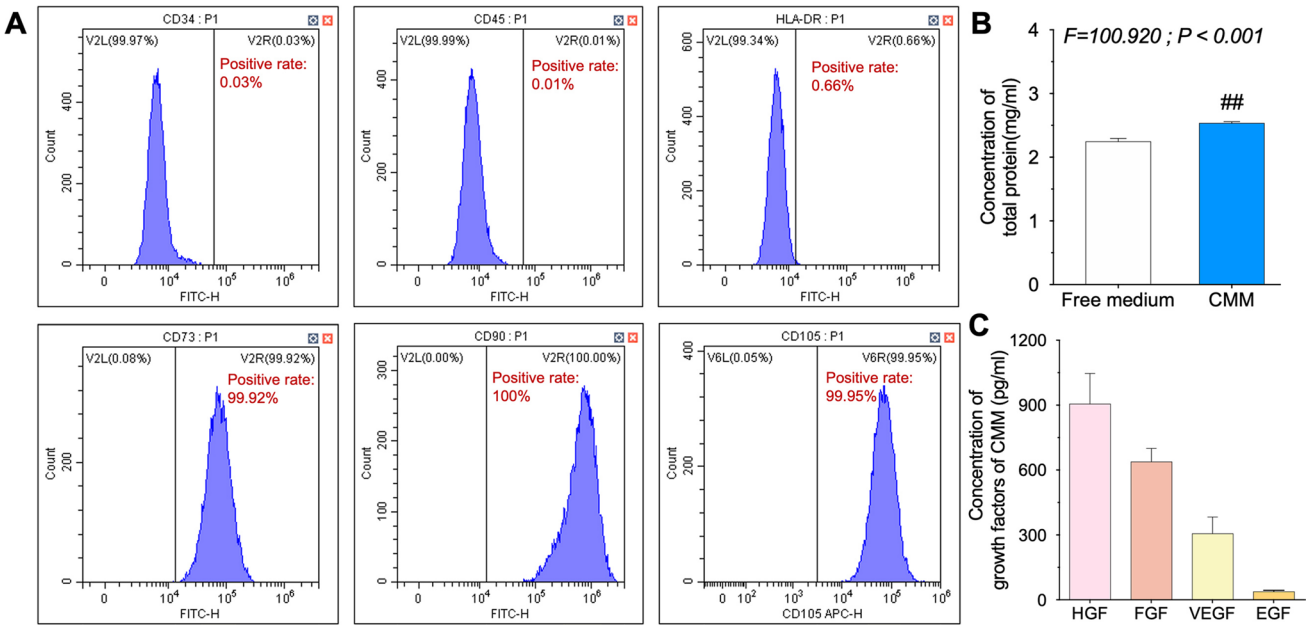


**Fig. 1** Identification of hucMSCs. The immunophenotype of hucMSCs surface markers determined by flow cytometry (**A**). Concentration of total protein of CMM and free medium (DMEM) (**B**). Concentrations of factors in CMM (**C**)

## Detection of ROS Level in HDFs by Flow Cytometry

The contents of ROS production in HDFs were examined using H2DCFDA. HDFs in different group were collected and incubated with 5 μM H2DCF-DA for 30 min at 37 °C with an atmosphere of 5% $CO_2$ in the dark. The cells were then washed with PBS and suspended in fresh medium, thereby detected by BD C6 flow cytometry (CA, USA). Flow cytometry was conducted according to the manufacturer's instruction.

## Real Time PCR

Real time PCR (qPCR) was employed to analyze the transcriptional expression of targeted genes by using ABI QuantStudio™ 7 Flex Real-Time PCR System (Applied Biosystems; Thermo Fisher Scientific, USA) as previously described [42]. Briefly, total RNA of HDFs was extracted by TRIzol reagent and quality controlled by NanoDrop2000 spectrophotometer (Thermo Scientific, USA). cDNA reverse transcription was performed by using All-in-One cDNA Synthesis SuperMix. $\beta$-actin was used as the reference gene and the $2^{-\Delta\Delta CT}$ method was used to analyze the relative mRNA expressions (Table 2).

## Autophagy Verification of CMM Mechanism

Chloroquine (CQ) was used to monitor autophagic flux for assessing autophagic activity [43]. HDFs were seeded onto 10 cm plates, followed treated with 2 μM CQ and CMM for 48 h. Four groups were designated as follows: NC group

**Table 3** Summary of RNA-seq data of hucMSCs and bioinformatics analysis of its paracrine factors [42, 44–66]

| Paracrine factors | Concentrations (pg/ml) | Regulated signaling pathways (KEGG analysis) | | | | |
|---|---|---|---|---|---|---|
| | | PI3K-Akt | MAPK | HIF-1 | NF-κB | JAK-STAT |
| VEGF | 3.3–3000 | * | * | | | |
| HGF | 30–2500 | * | * | | * | |
| TGF-β | 20–740.8 | | | | * | |
| BDNF | 500 | * | | | | |
| PDGF | 30–342.8 | * | * | | * | |
| FGF | 3.5–100 | * | * | * | * | |
| SCF | 3.2–25 | * | | | | |
| EGF | 2–6 | * | | * | * | * |
| IGF | 4 | * | * | * | * | |

* represents the regulation of paracrine factors

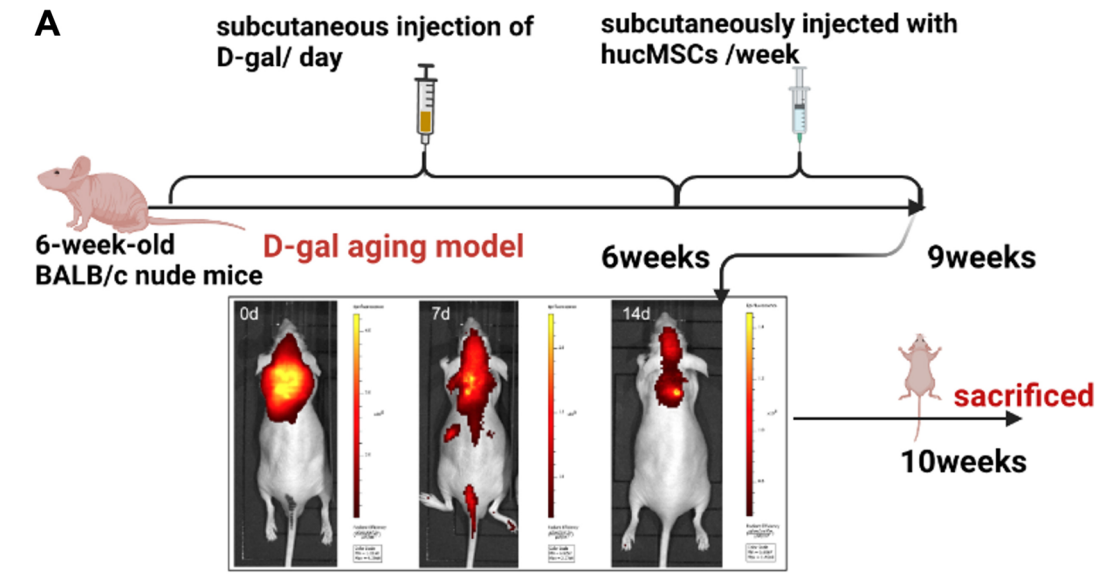
A
subcutaneous injection of
D-gal/ day
subcutaneously injected with
hucMSCs /week
6-week-old
BALB/c nude mice
D-gal aging model
6weeks
9weeks
0d
7d
14d
sacrificed
10weeks

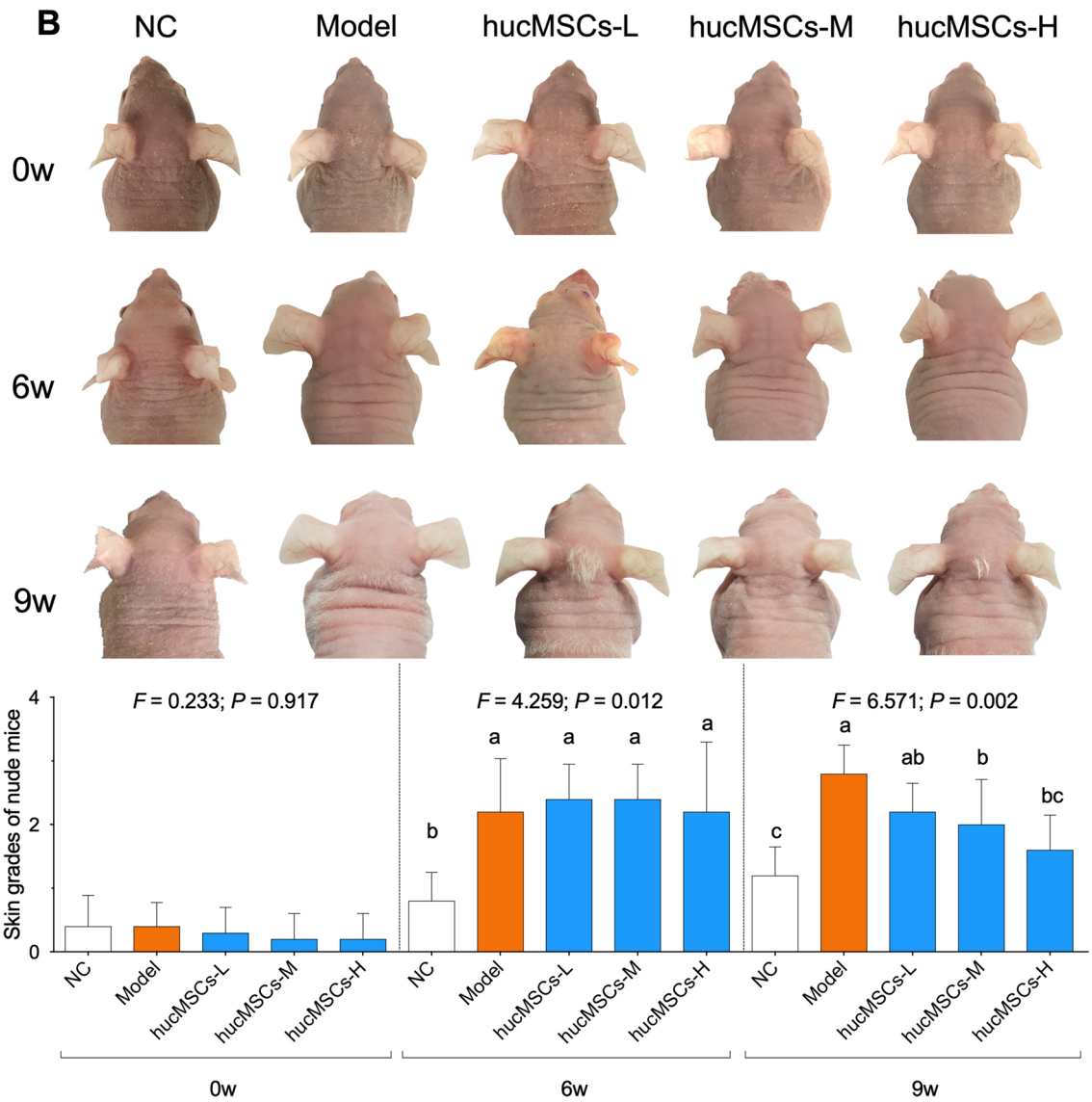
B
NC
Model
hucMSCs-L
hucMSCs-M
hucMSCs-H
0w
6w
9w
Skin grades of nude mice
F = 0.233; P = 0.917
F = 4.259; P = 0.012
F = 6.571; P = 0.002
a
ab
b
bc
c
0w
6w
9w

◂**Fig. 2** Study design of the animal experiment (**A**). Gross observation of skin appearance with estimation of skin grade of nude mice (**B**). Data expressed as mean ± SD (n = 5). Different symbols with overlapped letter (*e.g.* a *vs.* ab, bc *vs.* c) indicate statistical but not significant difference while different symbols with nonoverlapped letter (*e.g.* a *vs.* b, a *vs.* bc) indicate significant difference among groups [Fisher's least significant difference (LSD), $P < 0.05$]; the values decrease with the order from a to c

with no treatment, CMM group with CMM treatment, CQ group with CQ treatment, and CQ/CMM group with CQ plus CMM treatment. Western blot analysis was conducted to verify the changes of autophagy-related proteins. Rapamycin (500 nM) was added for autophagy activation and incubated with CMM treatment for 48 h. Six groups were designated as follows: NC group with no treatment, model group with D-gal treatment, CMM group with D-gal plus CMM treatment, rapamycin group with rapamycin treatment, D-gal/rapamycin group with D-gal plus rapamycin treatment, rapamycin/CMM group with D-gal plus rapamycin plus CMM treatment. Western blot analysis was conducted to verify the changes of autophagy-related proteins following rapamycin treatment. Each experiment was conducted in triplicate.

### Western Blot Analysis

Total proteins of HDFs were extracted with RIPA buffer with proteinase inhibitor cocktail for 30 min on ice. After 15 min centrifugation at 4 °C, the supernate was collected and the protein content was quantified by BCA protein quantification assay. The protein samples were separated by denaturing sodium dodecyl sulfate polyacrylamide gel electrophoresis (SDS-PAGE; 6–12%) and transferred onto a nitrocellulose membrane. The membrane was blocked with 5% non-fat milk for 2 h at 4 °C and followed by overnight incubation at 4 °C with primary antibodies against $\beta$-actin, p65, p-p65, p16, p21, LaminB1, HMGB1, p62 and LC3B.

After washing, the membrane was incubated with peroxidase-conjugated secondary antibodies at 4 °C for 2 h. Finally the results were visualized using Western Lightning® Plus ECL followed All proteins bands were detected by ECL kit (Biosharp, Beijing, China) and visualized by GE ImageQuant LAS4000 System 1 (Bio-Rad, Hercules, CA, USA). Results were analyzed with Image J software (version: 1.6.0). Each experiment was conducted in triplicate.

### Statistical Analysis

Data were expressed as the mean ± standard deviation. SPSS (version: 26.0) software was used to process the data. Data from different groups were compared with each other using one-way ANOVA assay, followed by Fisher's least significant difference (LSD) comparison. The $F$ value is the statistic of the F-test. A $P$ value $< 0.05$ was considered to indicate a significant difference and a $P$ value $< 0.01$ was considered to indicate a very significant difference.

## Results

### HucMSCs Identification

As shown in Fig. 1A, the umbilical cord-isolated cells expressed the surface markers CD73 (> 99%), CD90 (> 99%), and CD105 (> 99%), but not CD34 (< 0.1%), CD45 (< 0.1%) and HLA-DR (< 1%), which complied with the international standard of MSCs, indicating the cultured cells are qualified MSCs. As shown in Fig. 1B, concentration of total protein in the CMM was higher than that in free medium (DMEM) ($P < 0.01$), indicating that hucMSCs secreted potent substances through paracrine action. As shown in Table 3, we have summarized the published RNA-seq data of hucMSCs and collected the bioinformatics analysis of messages coding for paracrine factors. As shown in Fig. 1C, CMM contained high levels of HGF, FGF and VEGF, EGF was secreted at low level.

### In Vivo Efficacy of hucMSCs on Aged Skin of Nude Mice

To evaluate the anti-aging efficacy of hucMSCs on skin, D-gal-induced skin aging model was employed and subcutaneous injection of hucMSCs was performed for twice (once a week). As shown in Fig. 2A, the injected hucMSCs (stained by DiD dye) displayed remarkable fluorescent signal in the local injection site, and underwent gradual attenuation within three weeks. As shown in Fig. 2B, gross observation showed wider and deeper wrinkles of skin texture with higher skin grade in the model mice than that of NC mice after six weeks ($P < 0.01$). After hucMSCs treatment from low to high doses, the skin wrinkles of nude mice were gradually faded and the grades were statistically reduced in a dose-dependent manner when compared with the model ($P < 0.01$ for both middel and high doses of hucMSCs). Moreover, the grade with high-dose hucMSCs treatment was even close to the NC grade ($P > 0.05$).

### Biochemical, Histopathological and Immunofluorescence Analysis of Aged Skin with hucMSCs Treatment

Biochemical analysis on SOD and MDA was conducted to evaluate the anti-aging efficacy of hucMSCs in aspect of antioxidation. As shown in Fig. 3A, the SOD and MDA levels of the model skin were significantly altered when compared with the NC ($P < 0.01$), while hucMSCs from low to high doses significantly restored the alterations in a

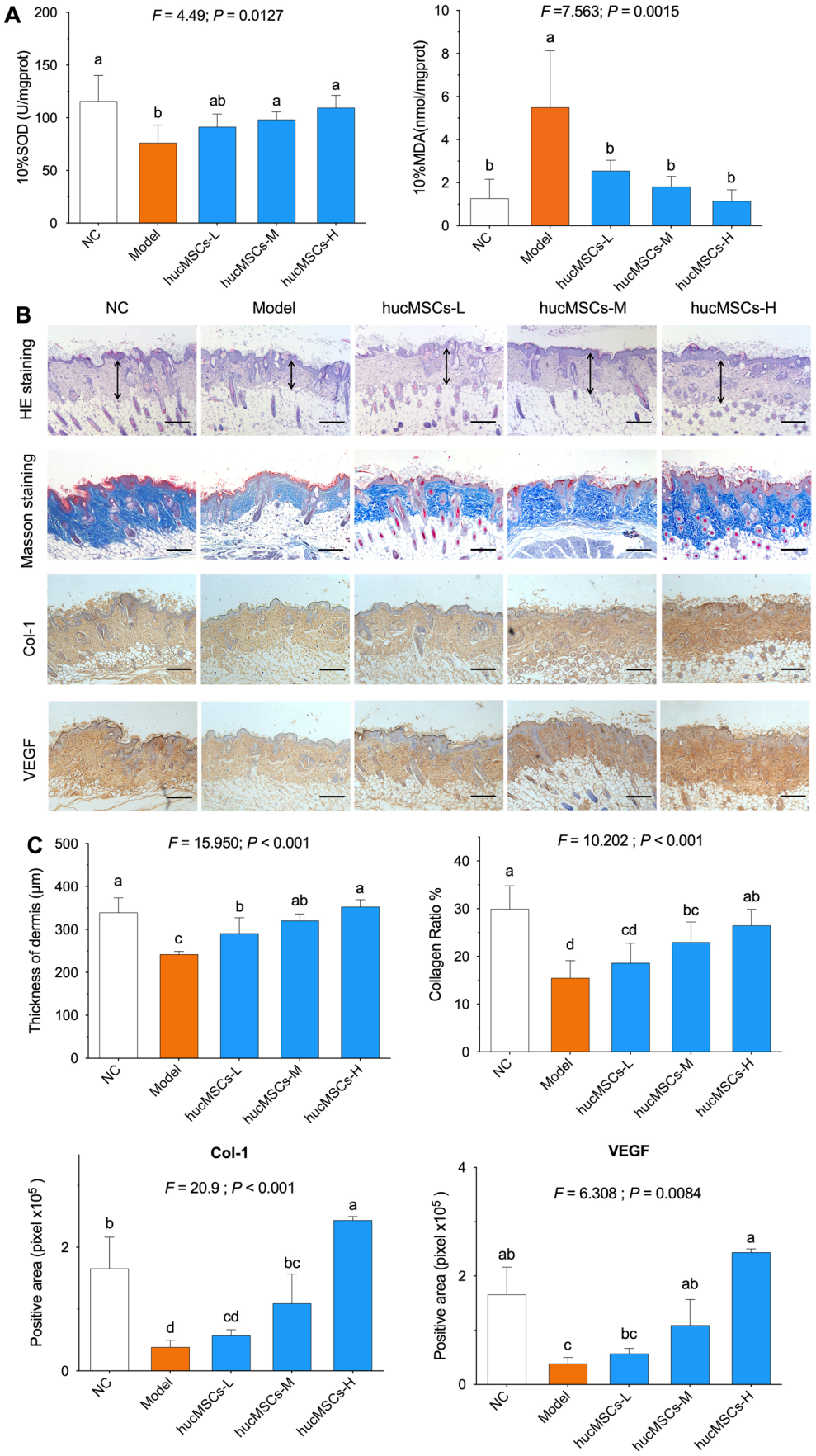
A
F = 4.49; P = 0.0127
10%SOD (U/mgprot)
F =7.563; P = 0.0015
10%MDA(nmol/mgprot)
NC
Model
hucMSCs-L
hucMSCs-M
hucMSCs-H
B
HE staining
Masson staining
Col-1
VEGF
C
F = 15.950; P < 0.001
Thickness of dermis (μm)
F = 10.202 ; P < 0.001
Collagen Ratio %
Col-1
F = 20.9 ; P < 0.001
Positive area (pixel x10^5)
VEGF
F = 6.308 ; P = 0.0084
Positive area (pixel x10^5)

◂**Fig. 3** SOD and MDA activities in skin of nude mice (**A**). Histopathological observation by HE and Masson staining, and immunohistochemical observation on Col-1 and VEGF expression (**B**). Statistical analysis of thickness of dermis, collagen ratio and positive area of Col-1 and VEGF expression (**C**). Scale bar = 200 μm. Data expressed as mean ± SD ($n = 5$). Different symbols with overlapped letter (*e.g.* a *vs.* ab, bc *vs.* c) indicate statistical but not significant difference while different symbols with nonoverlapped letter (*e.g.* a *vs.* b, a *vs.* bc) indicate significant difference among groups [Fisher's least significant difference (LSD), $P < 0.05$]; the values decrease with the order from a to c

dose-dependent manner (most $P < 0.01$). Exceptionally, hucMSCs at low dose statistically but not significantly restored the SOD level in comparison with the model level ($P > 0.05$). Histopathological observation was conducted to evaluate the anti-aging efficacy of hucMSCs on dermal thickness and collagen fibers of aged skin. As shown in Fig. 3B (upper) and 3C (upper), both HE and Masson′s trichrome staining showed significant decrease of dermal thickness and loss of collagen fibers in the model skin when compared with the NC skin ($P < 0.01$). In contrast, the histopathological abnormalities were restored with significant increase of dermal thickness and production of collagen fibers by hucMSCs in a dose-dependent manner ($P < 0.01$ *vs.* model).

Col-1 and VEGF are key markers of dermis, which are related to the ECM rengeration and state of HDFs. Immunohistochemical staining was applied to visualize the expression of Col-1 and VEGF in dermal extracellular matrix. As shown in Fig. 3B (lower) and 3C (lower), the expression of Col-1 and VEGF (positive area) were significantly decreased in the model group ($P < 0.01$ *vs*. NC) but were statistically restored to normal levels in the hucMSCs groups ($P < 0.01$ *vs*. model for hucMSCs-M and hucMSCs-H). Moreover, such regulatory effect of hucMSCs on Col-1 and VEGF was dose-dependent.

## In Vitro Paracrine Effects of hucMSCs on Senescent HDFs

D-gal-induced senescence model of HDFs was established and the in vitro effects of CMM was evaluated by wound healing assay, SA-β-gal staining, and ROS sensitive probe H2DCFDA to determine the paracrine action of hucMSCs on senescent HDFs. As shown in Fig. 4A, the wound area ratios (24 h of 0 h and 48 h of 0 h) of model HDFs were significantly higher than that of NC HDFs (both $P < 0.01$), while CMM significantly restored the wound area ratios (both $P < 0.01$ *vs.* model). More importantly, the CMM treatment even resulted in better outcomes of wound healing than NC at 24 and 48 h. As shown in Fig. 4B, the number of SA-β-gal stained senescent HDFs (in azure blue color) was significantly increased in the model group ($P < 0.01$ *vs.* NC) and was significantly decreased in the CMM-treated group ($P < 0.01$ *vs.* model). ROS sensitive probe H2DCFDA and flow cytometry were applied to assess the ROS level in HDFs. As shown in Fig. 4C, the ROS level in the model group was significantly higher than that of NC group ($P < 0.01$), and that in the CMM group was significantly decreased to NC level ($P < 0.01$ *vs.* model). The above data indicated that hucMSCs exerted in vitro paracrine effects on senescent HDFs by improving wound healing, inhibiting cell senescence and suppressing ROS production.

## Molecular Actions of CMM on Senescent HDFs

qPCR and WB analyses were conducted to elucidate the molecular actions of CMM on senescent HDFs. As shown in Fig. 5A, the mRNA expressions of *p16, p21*, *p65*, *IL-6*, *MMP1* and *MMP3* were significantly up-regulated and that of *Col-1* and *SOD1* was significantly down-regulated in the model HDFs ($P < 0.05$ or 0.01 *vs.* NC). The abnormal changes of these genes were significantly restored by CMM toward NC levels after 48 treatment ($P < 0.01$ *vs.* model). As shown in Fig. 5B, the protein expressions of p65, p-p65, p16, p21 and HMGB1 were significantly up-regulated and that of LaminB1, p62 and LC3B were significantly down-regulated in the model HDFs (all $P < 0.01$ *vs.* NC). In contrast, CMM significantly restored the abnormal expressions of these proteins toward NC levels (all $P < 0.01$ *vs.* model). The above data suggested that CMM acted on HDFs by modulating autophagy-related and senescence-related molecules.

## Verification of Autophagy-Related Mechanism of CMM

The autophagy inhibitor (CQ) and promoter (rapamycin) were applied to verify the autophagy-related mechanism of CMM. One of the principal methods in current use to measure autophagic flux is the monitoring of LC3 turnover, which is based on the observation that LC3B-II is degraded in autolysosomes [43]. As shown in Fig. 6A, HDFs are treated with CQ, the degradation of LC3B-II is blocked, resulting in the accumulation of LC3B-II. The difference in LC3-II levels in the presence and absence of CQ is smaller under CMM treatment (compare CMM group and CQ/CMM group), indicating that CMM treatment reduced autophagic flux and inhibit the autophay. Moreover, the total cellular expression levels of p62 inversely correlate with autophagic activity. As shown in Fig. 6B, the protein expressions of LaminB1 and p16 were altered by model group ($P < 0.01$ *vs.* NC) and restored by CMM group ($P < 0.01$ *vs.* Model). With rapamycin treatment, the expression of LaminB1 was decreased and p16 was increased (all $P < 0.01$). Moreover, the CMM-induced alterations were completely blocked by rapamycin in the rapamycin/CMM group, when compared with the CMM group (all $P < 0.01$ *vs.* CMM). Therefore, these data indicated that CMM exerted anti-aging effect by inhibiting autophagy.

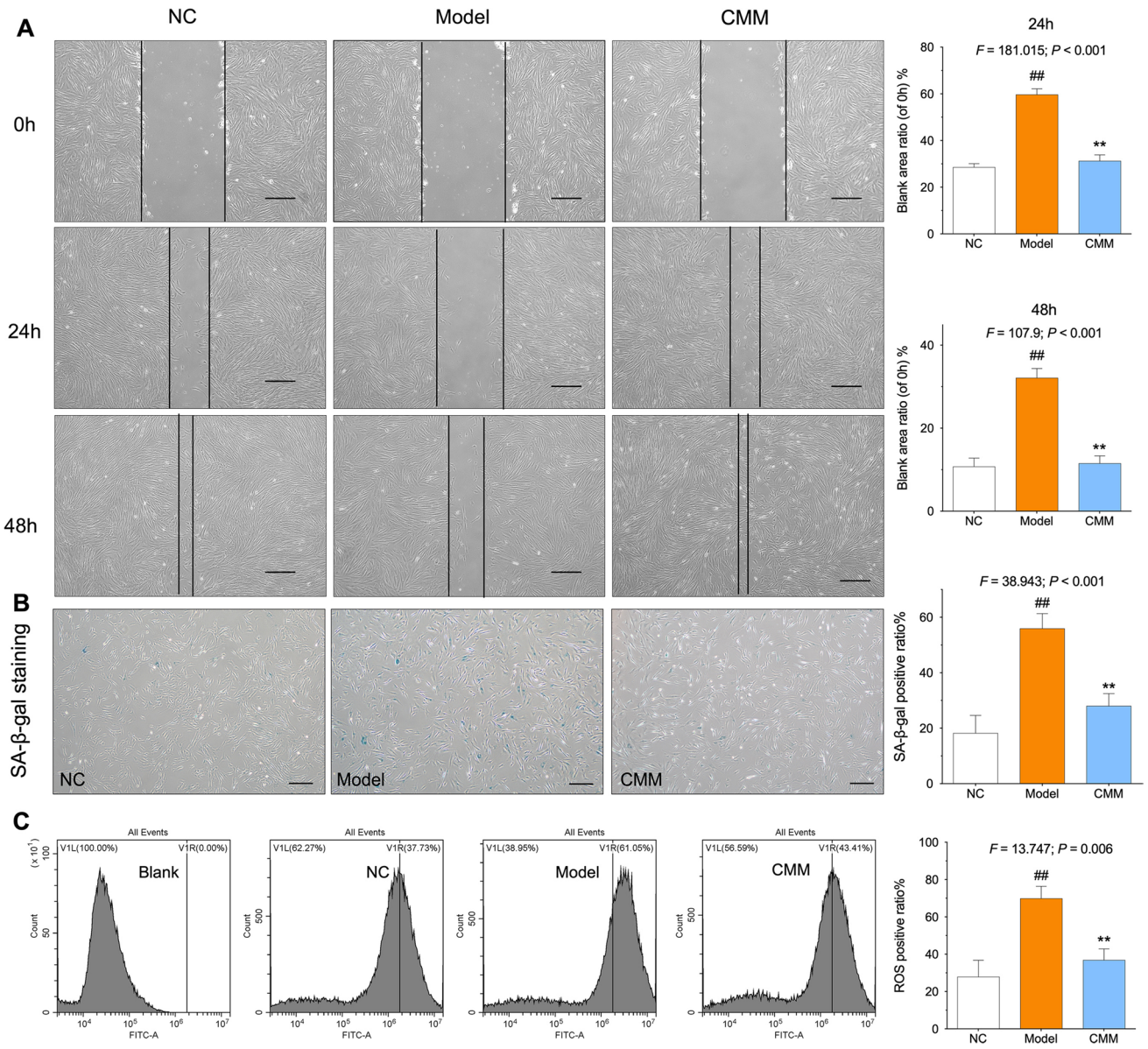


**Fig. 4** Wounding healing assay of HDFs with wound area ratio statistical analysis at 0 h, 24 h and 48 h (**A**). SA-β-gal staining of HDFs and scoring of the SA-β-gal positive cells number (**B**). ROS level of HDFs and scoring of the ROS positive ratio (**C**). Scale bar = 200 μm. Data expressed as mean ± SD ($n = 3$). $^{\#\#}P < 0.01$ *vs.* NC; $^{*}P < 0.05$ or $^{**}P < 0.01$ *vs.* model by one-way ANOVA followed by LSD multiple comparison

## Discussion

Although several kinds of MSCs have been reported to improve the tissue repair and regeneration, the efficacy and mechanism of hucMSCs on skin aging remain poorly understood [67]. By using nude mice model and HDFs, this study was conducted to bridge this gap and eventually evidenced the efficacy and mechanism of hucMSCs on skin aging. The animal data demonstrated that hucMSCs dose-dependently removed wrinkles, smoothed skin texture, and increased dermal thickness and ECM collagen production of aged skin by reversing the levels of SOD and MDA and the abnormal expressions of Col-1 and VEGF, indicating anti-oxidative and pro-regenerative effects of hucMSCs on skin aging (Figs. 2 and 3). The cellular data demonstrated that MSCs-CM restored the senescence of HDFs by inhibiting the ROS production, improving the cell migration, and reversing the overexpressions of oxidative and senescent genes (Figs. 4 and 5), and the underlying paracrine mechanism was clarified as autophagy inhibition (Fig. 6). MSCs-CM was the most frequently used form of stem cell secretome to study the paracrine action of MSCs, containing

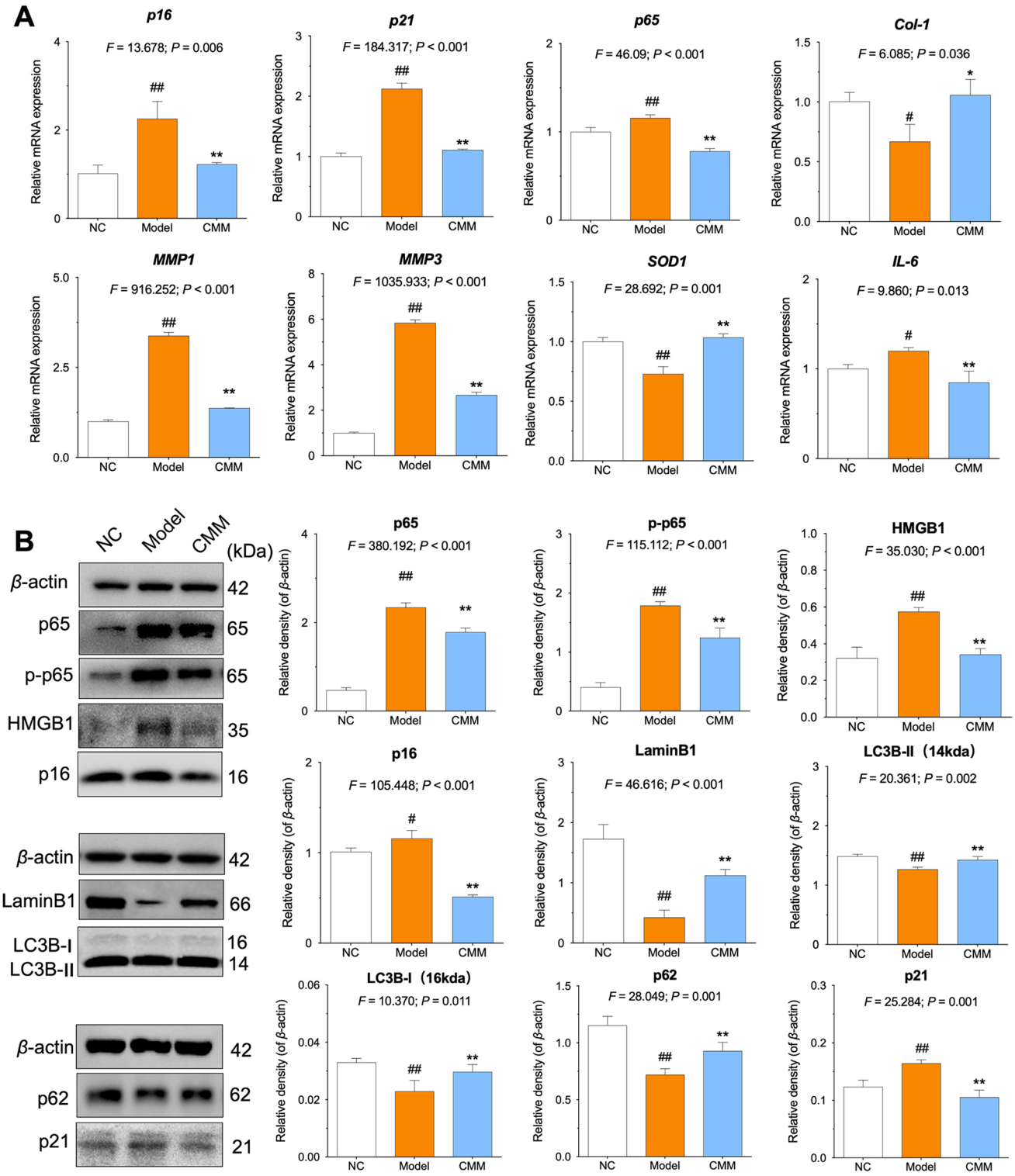


**Fig. 5** The relative mRNA expressions of senescence-related genes of HDFs with CMM treatment (**A**). Protein bands and protein expressions of autophagy-related and senescence-related molecules in HDFs with CMM treatment (**B**). Data expressed as mean ± SD ($n = 3$). $^{\#\#}P < 0.05$ or $^{\#\#}P < 0.01$ *vs.* NC group; $^{*}P < 0.05$ or $^{**}P < 0.01$ *vs.* model group by one-way ANOVA followed by LSD multiple comparison

platelet-derived growth factor (PDGF), cell growth-stimulating factor (C-GSF), stromal-derived factor-1 (SDF-1), HGF, VEGF, growth differentiation factor 11 (GDF11), transforming growth factor (TGF-β), insulin-like growth factor (IGF), etc. [68, 69]. These factors have potential in tissue repair and regeneration [68, 69]. Of these, GDF11 and TGF-β in ADSCs secretome contributed to the proliferation of HDFs and improvement of skin structure [70], and C-GSF in human amniotic MSCs secretome and VEGF and HGF in BMSCs secretome exerted anti-inflammatory, pro-migrative and proliferative effects on skin tissue [71, 72]. In this study, we have summarized the published RNA-seq data of hucMSCs and collected the bioinformatics analysis of messages coding for paracrine factors. As shown in Table 3, hucMSCs secreted a variety of paracrine factors, mainly including VEGF, HGF, TGF-β, BDNF, PDGF, FGF, SCF, EGF and IGF, which possessed functions in association with various paracrine signalings. Of these, VEGF, HGF, BDNF, PDGF, FGF, SCF, EGF and IGF could activate PI3K-Akt signaling pathway that promoted cell proliferation, angiogenesis and DNA repair against cellular senescence [44, 45, 48, 53, 57, 59, 63], FGF, EGF, and IGF could activate HIF-1 signaling pathway that enhanced proliferation of epidermal keratinocytes and improved regeneration of new collagen, elastin, and blood vessels [61, 64, 66], and EGF could stimulate proliferation and migration of wounded cells via the JAK/STAT pathway [65]. Besides, VEGF, HGF, PDGF, FGF and IGF could act on MAPK signaling pathway that participated in oxidative stress-induced skin aging [53, 54, 58, 60], and HGF, TGF-β, PDGF, FGF, EGF and IGF could inhibit NF-κB signaling pathway that facilitated skin aging, inflammation and cellular senescence [42, 55, 62]. In this study, we found the presence of HGF, FGF, VEGF and EGF in our CMM (Fig. 1C), indicating those paracrine factors as the main contributor to hucMSCs′ anti-aging efficacy. Further studies are warranted for exploring the concrete roles and contributions of those paracrine factors in hucMSCs. In sum, the innovation of this study could thereby be proposed as: 1) determination of rejuvenative efficacy and mechanism of hucMSCs on skin aging; 2) clarification of autophagy-mediated paracrine mechanism of hucMSCs on senescent HDFs.

Increased oxidative stress, activated cellular senescence, and lacked ECM regeneration are main contributors to skin aging. ROS, SOD, and MDA are key markers of oxidative stress, representing the anti-oxidative effect of treatment against aging. Of these, ROS is a by-product in the electron transport chain of aerobic cellular metabolism, resulting in intrinsic aging with DNA damage and oxidative stress [73]. ROS induces production of MDA, a lipid peroxidation product, further leading to cellular senescence and ECM damage [74]. On the contrary, SOD acts as an anti-oxidative enzyme to maintain the redox homeostasis by scavenging ROS, supporting the matrix composition and thickness of

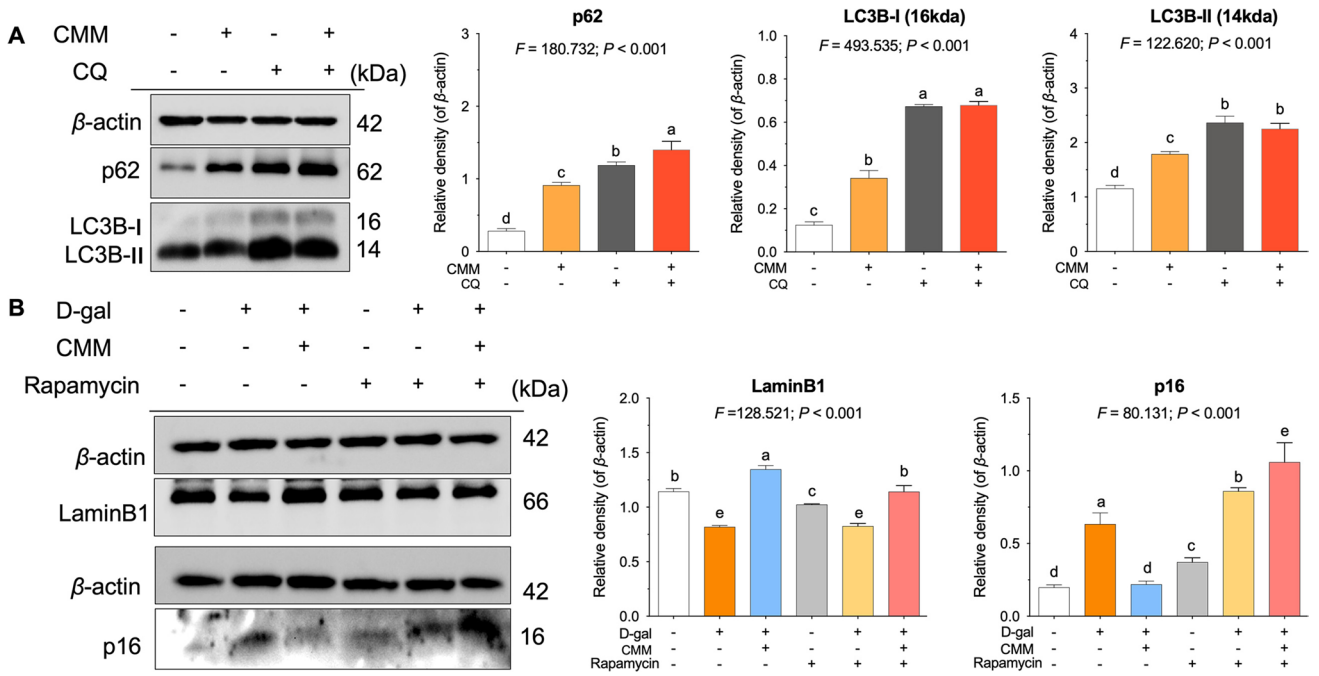


**Fig. 6** Protein bands and protein expressions of HDFs with CMM plus CQ treatment (**A**). Protein bands and protein expressions of HDFs with D-gal, CMM and rapamycin treatment (**B**). Data expressed as mean ± SD ($n = 3$). Different symbols (a, b, c, d and e) indicate significant difference among groups [Fisher's least significant difference (LSD), $P < 0.05$], and the values decrease with the order from a to e

skin [73, 75–77]. Cellular senescence is another key contributor to skin aging, which characterized by secretion of senescence-associated secretory proteins (SASP). Increased β-galactosidase activity is the typical phenotype of senescence, associated with increased expressions of cyclin-dependent kinase inhibitors, such as p16 (CDKN2A) and p21(CDKN1A), leading to cell cycle arrest [78]. In SASP, MMPs are produced by HDFs and play key roles in degrading ECM and accelerating skin aging, MMP1 and MMP3 of which acts as collagenase and stromelysin, respectively [79]. Besides, LaminB1 and HMGB1 are senescence markers that trigger or accelerate aging process through proinflammation [80, 81]. In the skin dermal ECM, Col-1 is the main component accounting for 80% of the total collagen fibers that confers mechanical strength and elasticity to skin, and VEGF functions to induce not only angiogenesis but also proliferation and migration of HDFs, benifiting regeneration of dermal ECM [82–84]. In this study, the above parameters were all altered by the aging modeling and were restored by hucMSCs, indicating that hucMSCs exerted anti-aging efficacy on skin through inhibition of oxidative stress, suppression of cellular senescence, and promotion of ECM regeneration.

This study clarified that autophagy mediated the anti-aging mechanism of hucMSCs, in which autophagy negatively regulated the senescence of HDFs. As a lysosome-dependent degradation process, autophagy is activated by cellular stresses, such as anoxia, DNA damage, and peroxidation (excessive ROS), and participates in the pathogenesis of aging [85–87]. During autophagy, the substrates (damaged organelles, cytosolic proteins and invasive microbes) are sequestered within double-membraned vesicles, known as autophagosomes, which eventually fuse with lysosomes and thereby result in degradation of the contents [88]. LC3 is an important marker of autophagy and the turnover of LC3 can be used for assessing general autophagic flux [89]. In the cytoplasm, deacetylated LC3B-I is lipidated by conjugation with phosphatidylethanolamine and then converted to LC3B-II, being recruited by autophagosomes [89, 90]. The adaptor protein p62 is another marker of autophagy, which selectively incorporates into autophagosomes by binding to LC3 and then degraded with autophagy [43]. Depletion of p62 results in the increased abundance of GATA4 protein, the senescence regulator, triggering NF-κB activation and SASP secretion to accelerate senescence [91]. In this study, autophagy was activated with overexpression and phosphorylation of p65 as well as LC3 turnover in senescent HDFs, whereas hucMSCs reversed the above alterations through paracrine action, indicating that autophagy suppression was the anti-aging mechanism of hucMSCs on skin (Figs. 5 and 6). Our finding was consistent with previous study that autophagy was activated upon the acute induction of senescence and played a critical role in the mitotic/transition phase of cellular senescence [92]. Moreover, LaminB1 was down-regulated in senescent cells with activation of autophagy/lysosomal pathway, contributing to the senescent state [78]. It has also been reported that activation of autophagosome was involved in UVB-induced senescence of HDFs and the basal level of autophagy was increased during replication of senescent HDFs, which depended on accumulation of ROS [93, 94].

## Conclusions

This study demonstrated rejuvenative efficacy of hucMSCs on skin aging and clarified the autophagy related anti-aging mechanism of this stem cell therapy. In vivo, hucMSCs removed wrinkles and smoothened skin texture by exerting antioxidative and rengerative effects on skin ECM. In vitro, hucMSCs exerted anti-senescent and beneficial effects on HDFs by inhibiting oxidative stress, suppressing cellular senescence, and promoting cell migration, in paracrine-based manner. The anti-senescent paracrine mechanism of hucMSCs was the inhibition of autophagy in senescent HDFs. Therefore, hucMSCs may be a promising candidate of stem cell therapy for anti-aging treatment, and moreover, hucMSCs-CM may be an useful substitute of hucMSCs. Altogether, this study provided novel knowledge of MSCs in treating skin aging, which was significant for the development of stem cell therapy in clinic.

**Abbreviations** MSCs: Mesenchymal stem cells; hucMSCs: Human umbilical cord-derived mesenchymal stem cells; CMM: Conditional medium of human umbilical cord-derived mesenchymal stem cells; HDFs: Human dermal fibroblasts; SA-β-gal: Senescence-associated-beta-galactosidase; ECM: Extracellular matrix; ROS: Reactive oxygen species; MMPs: Matrix metalloproteinase; SOD: Superoxide dismutase; MDA: Malondialdehyde; D-gal: D-Galactose; mRNA: Messenger ribonucleic acid; SASP: Senescence-associated secretory phenotype; Col-1: Collagen I; VEGF: Vascular endothelial growth factor; NF-κB: Nuclear factor kappa-B; CQ: Chloroquine; ATG5: Autophagy protein 5; LC3: Microtubule- associated proteins light chain 3; FBS: Fatal Bovine Serun; PBS: Phosphate Buffered Saline; PVDF: Polyvinylidene fluoride; RT-PCR: Real-Time Polymerase Chain Reaction; SDS-PAGE: Sodium dodecyl sulfate polyacrylamide gel electrophoresis; BSA: Bovine Serum Albumin; TBS: Tris Buffered Saline; TBST: Tris Buffered saline Tween; WB: Western Blot; PDGF: Platelet-derived growth factor; C-GSF: Cell growth-stimulating factor; GDF11: Cell growth-stimulating factor; IGF: Insulin-like growth factor; HGF: Hepatocyte growth factor; TGF-β: Transforming growth factor; SCF: Stem cell factor; BDNF: Brain-derived neurotrophic factor; FGF: Fibroblast growth factor; EGF: Epidermal growth factor

**Authors' Contributions** Ting Li conducted the main work of this study; Li Zhou contributed to the mechanism study of hucMSCs; Mengqiang Fan contributed to the animal experiments of this study; Zuxiang Chen improved the experimental design and methodology; Li Yan improved the experimental methodology; Haishan Lu and Ming Jia contributed to the funding support of this study; Huiling Wu provided ideas, designed and funded this study; Letian Shan designed, drafted and funded this study.

**Funding** This work was supported by Zhejiang Provincial Basic Public Welfare Research Program (Grant No. LGF18H110003 from Haishan Lu and Grant No. LGF22H150017 from Huiling Wu) for materials of experiments, Zhejiang Provincial Natural Science Foundation of China (Grant No. LQ20H150008) and Hangzhou Science and Technology Development Program (Grant No. 20180533B38 from Ming Jia) for collection and interpretation of data.

**Data Availability** The data that support the findings of this study are available from the corresponding author upon reasonable request.

**Code Availability** Not applicable.

## Declarations

**Ethics Approval** All experiments on the mice were approved by the Medical Norms and Ethics Committee of Zhejiang Chinese Medical University.

**Consent to Participate** Not applicable.

**Consent for Publication** All authors have approved this submission and publication.

**Conflicts of Interest** The authors have declared that no competing interest exists.

## References

1. Todorova, K., & Mandinova, A. (2020). Novel approaches for managing aged skin and nonmelanoma skin cancer. *Advanced Drug Delivery Reviews, 153*, 18–27.
2. Sies, H., Berndt, C., & Jones, D. P. (2017). Oxidative Stress [in eng]. *Annual Review of Biochemistry, 86*, 715–748.
3. Kammeyer, A., & Luiten, R. M. (2015). Oxidation events and skin aging. *Ageing Research Reviews, 21*, 16–29.
4. Gu, Y., Han, J., Jiang, C., et al. (2020). Biomarkers, oxidative stress and autophagy in skin aging. *Ageing Research Reviews, 59*, 101036.
5. Wlaschek, M., Maity, P., Makrantonaki, E., et al. (2021). Connective Tissue and Fibroblast Senescence in Skin Aging. *The Journal of Investigative Dermatology, 141*(4S), 985–992.
6. Naylor, E. C., Watson, R. E., & Sherratt, M. J. (2011). Molecular aspects of skin ageing. *Maturitas, 69*(3), 249–256.
7. Lephart, E. D. (2016). Skin aging and oxidative stress: Equol's anti-aging effects via biochemical and molecular mechanisms. *Ageing Research Reviews, 31*, 36–54.
8. Lohakul, J., Jeayeng, S., Chaiprasongsuk, A. et al. (2021). Mitochondria-Targeted Hydrogen Sulfide Delivery Molecules Protect Against UVA-Induced Photoaging in Human Dermal Fibroblasts, and in Mouse Skin In Vivo. *Antioxid Redox Signal*.
9. Boo, Y. C. (2019). Human Skin Lightening Efficacy of Resveratrol and Its Analogs: From in Vitro Studies to Cosmetic Applications. *Antioxidants (Basel)*, *8*(9).
10. Baumann, L. (2007). Skin ageing and its treatment. *The Journal of Pathology, 211*(2), 241–251.
11. Wang, L., Lee, W., Cui, Y. R., et al. (2019). Protective effect of green tea catechin against urban fine dust particle-induced skin aging by regulation of NF-kappaB, AP-1, and MAPKs signaling pathways. *Environmental Pollution, 252*(Pt B), 1318–1324.
12. Gruber, F., Ornelas, C. M., Karner, S., et al. (2015). Nrf2 deficiency causes lipid oxidation, inflammation, and matrix-protease expression in DHA-supplemented and UVA-irradiated skin fibroblasts. *Free Radical Biology & Medicine, 88*(Pt B), 439–451.
13. Eckhart, L., Tschachler, E., & Gruber, F. (2019). Autophagic Control of Skin Aging. *Front Cell Dev Biol, 7*, 143.
14. Gerland, L. M., Peyrol, S., Lallemand, C., et al. (2003). Association of increased autophagic inclusions labeled for beta-galactosidase with fibroblastic aging. *Experimental Gerontology, 38*(8), 887–895.
15. Gewirtz, D. A. (2013). Autophagy and senescence: A partnership in search of definition. *Autophagy, 9*(5), 808–812.
16. Liu, H., He, Z., von Rutte, T. et al. (2013). Down-regulation of autophagy-related protein 5 (ATG5) contributes to the pathogenesis of early-stage cutaneous melanoma. *Science Translational Medicine*, *5*(202), 202ra123.
17. Roh, E., Kim, J. E., Kwon, J. Y., et al. (2017). Molecular mechanisms of green tea polyphenols with protective effects against skin photoaging. *Critical Reviews in Food Science and Nutrition, 57*(8), 1631–1637.
18. Kim, J., Kim, J., Lee, Y. I., et al. (2020). Effect of a topical antioxidant serum containing vitamin C, vitamin E, and ferulic acid after Q-switched 1064-nm Nd:YAG laser for treatment of environment-induced skin pigmentation. *Journal of Cosmetic Dermatology, 19*(10), 2576–2582.
19. Woodby, B., Penta, K., Pecorelli, A., et al. (2020). Skin Health from the Inside Out. *Annual Review of Food Science and Technology, 11*, 235–254.
20. Valacchi, G., Pecorelli, A., Belmonte, G., et al. (2017). Protective Effects of Topical Vitamin C Compound Mixtures against Ozone-Induced Damage in Human Skin. *The Journal of Investigative Dermatology, 137*(6), 1373–1375.
21. Walle, T. (2011). Bioavailability of resveratrol. *Annals of the New York Academy of Sciences, 1215*, 9–15.
22. OyetakinWhite, P., Tribout, H., & Baron, E. (2012). Protective mechanisms of green tea polyphenols in skin. *Oxidative Medicine and Cellular Longevity, 2012*, 560682.
23. Rinaldi, F. (2008). Laser: A review [in eng]. *Clinics in Dermatology, 26*(6), 590–601.
24. Weiss, R. A., McDaniel, D. H., Geronemus, R. G. (2003). Review of nonablative photorejuvenation: reversal of the aging effects of the sun and environmental damage using laser and light sources [in eng]. *Seminars in Cutaneous Medicine and Surgery*, *22*(2).
25. Si, Y.-L., Zhao, Y.-L., Hao, H.-J. et al. (2011). MSCs: Biological characteristics, clinical applications and their outstanding concerns [in eng]. *Ageing Research Reviews*, *10*(1).
26. Pittenger, M. F., Mackay, A. M., Beck, S. C., et al. (1999). Multilineage potential of adult human mesenchymal stem cells. *Science, 284*(5411), 143–147.
27. Wang, Y., Chen, X., Cao, W., et al. (2014). Plasticity of mesenchymal stem cells in immunomodulation: Pathological and therapeutic implications. *Nature Immunology, 15*(11), 1009–1016.
28. Kong, P., Xie, X., Li, F., et al. (2013). Placenta mesenchymal stem cell accelerates wound healing by enhancing angiogenesis in diabetic Goto-Kakizaki (GK) rats. *Biochemical and Biophysical Research Communications, 438*(2), 410–419.

29. Son, W. C., Yun, J. W., & Kim, B. H. (2015). Adipose-derived mesenchymal stem cells reduce MMP-1 expression in UV-irradiated human dermal fibroblasts: Therapeutic potential in skin wrinkling. *Bioscience, Biotechnology, and Biochemistry, 79*(6), 919–925.
30. Lai, P., Chen, X., Guo, L., et al. (2018). A potent immunomodulatory role of exosomes derived from mesenchymal stromal cells in preventing cGVHD. *Journal of Hematology & Oncology, 11*(1), 135.
31. De Gregorio, C., Contador, D., Diaz, D., et al. (2020). Human adipose-derived mesenchymal stem cell-conditioned medium ameliorates polyneuropathy and foot ulceration in diabetic BKS db/db mice. *Stem Cell Research & Therapy, 11*(1), 168.
32. Lee, D. E., Ayoub, N., & Agrawal, D. K. (2016). Mesenchymal stem cells and cutaneous wound healing: Novel methods to increase cell delivery and therapeutic efficacy. *Stem Cell Research & Therapy, 7*, 37.
33. El Omar, R., Beroud, J., Stoltz, J. F., et al. (2014). Umbilical cord mesenchymal stem cells: The new gold standard for mesenchymal stem cell-based therapies? *Tissue Engineering. Part B, Reviews, 20*(5), 523–544.
34. Bartolucci, J., Verdugo, F. J., Gonzalez, P. L., et al. (2017). Safety and Efficacy of the Intravenous Infusion of Umbilical Cord Mesenchymal Stem Cells in Patients With Heart Failure: A Phase 1/2 Randomized Controlled Trial (RIMECARD Trial [Randomized Clinical Trial of Intravenous Infusion Umbilical Cord Mesenchymal Stem Cells on Cardiopathy]). *Circulation Research, 121*(10), 1192–1204.
35. Nagamura-Inoue, T., & He, H. (2014). Umbilical cord-derived mesenchymal stem cells: Their advantages and potential clinical utility [in eng]. *World J Stem Cells, 6*(2), 195–202.
36. Barcia, R. N., Santos, J. M., Teixeira, M., et al. (2017). Umbilical cord tissue-derived mesenchymal stromal cells maintain immunomodulatory and angiogenic potencies after cryopreservation and subsequent thawing. *Cytotherapy, 19*(3), 360–370.
37. Quimby, J. M., Webb, T. L., Habenicht, L. M., et al. (2013). Safety and efficacy of intravenous infusion of allogeneic cryopreserved mesenchymal stem cells for treatment of chronic kidney disease in cats: Results of three sequential pilot studies. *Stem Cell Research & Therapy, 4*(2), 48.
38. Thomi, G., Surbek, D., Haesler, V., et al. (2019). Exosomes derived from umbilical cord mesenchymal stem cells reduce microglia-mediated neuroinflammation in perinatal brain injury. *Stem Cell Research & Therapy, 10*(1), 105.
39. Yang, J., Chen, Z., Pan, D., et al. (2020). Umbilical Cord-Derived Mesenchymal Stem Cell-Derived Exosomes Combined Pluronic F127 Hydrogel Promote Chronic Diabetic Wound Healing and Complete Skin Regeneration. *International Journal of Nanomedicine, 15*, 5911–5926.
40. Matas, J., Orrego, M., Amenabar, D., et al. (2019). Umbilical Cord-Derived Mesenchymal Stromal Cells (MSCs) for Knee Osteoarthritis: Repeated MSC Dosing Is Superior to a Single MSC Dose and to Hyaluronic Acid in a Controlled Randomized Phase I/II Trial [in eng]. *Stem Cells Translational Medicine, 8*(3), 215–224.
41. Umbayev, B., Askarova, S., Almabayeva, A., et al. (2020). Galactose-Induced Skin Aging: The Role of Oxidative Stress. *Oxidative Medicine and Cellular Longevity, 2020*, 7145656.
42. Li, T., Lu, H. S., Zhou, L. et al. (2022). Growth factors-based platelet lysate rejuvenates skin against ageing through NF-kappa B signalling pathway: In vitro and in vivo mechanistic and clinical studies [in English]. *Cell Proliferation*, *55*(4).
43. Mizushima, N., Yoshimori, T., & Levine, B. (2010). Methods in mammalian autophagy research. *Cell, 140*(3), 313–326.
44. Zhang, Z., Li, Z., Wang, Y., et al. (2021). PDGF-BB/SA/Dex injectable hydrogels accelerate BMSC-mediated functional full thickness skin wound repair by promoting angiogenesis. *J Mater Chem B, 9*(31), 6176–6189.
45. Guo, S., Wang, T., Zhang, S. Y., et al. (2020). Adipose-derived stem cell-conditioned medium protects fibroblasts at different senescent degrees from UVB irradiation damages [in English]. *Molecular and Cellular Biochemistry, 463*(1–2), 67–78.
46. Park, Y. M., Lee, M., Jeon, S., et al. (2021). In vitro effects of conditioned medium from bioreactor cultured human umbilical cord-derived mesenchymal stem cells (hUC-MSCs) on skin-derived cell lines. *Regen Ther, 18*, 281–291.
47. Guo, Z. Y., Sun, X., Xu, X. L., et al. (2015). Human umbilical cord mesenchymal stem cells promote peripheral nerve repair via paracrine mechanisms. *Neural Regeneration Research, 10*(4), 651–658.
48. Jiao, W., Mi, X., Yang, Y., et al. (2022). Mesenchymal stem cells combined with autocrosslinked hyaluronic acid improve mouse ovarian function by activating the PI3K-AKT pathway in a paracrine manner. *Stem Cell Research & Therapy, 13*(1), 49.
49. Xin, L., Lin, X., Pan, Y., et al. (2019). A collagen scaffold loaded with human umbilical cord-derived mesenchymal stem cells facilitates endometrial regeneration and restores fertility. *Acta Biomaterialia, 92*, 160–171.
50. Yi, X., Chen, F., Liu, F., et al. (2020). Comparative separation methods and biological characteristics of human placental and umbilical cord mesenchymal stem cells in serum-free culture conditions. *Stem Cell Research & Therapy, 11*(1), 183.
51. Dabrowski, F. A., Burdzinska, A., Kulesza, A., et al. (2017). Comparison of the paracrine activity of mesenchymal stem cells derived from human umbilical cord, amniotic membrane and adipose tissue [in English]. *J Obstet Gynaecol Re, 43*(11), 1758–1768.
52. Gabrielyan, A., Quade, M., Gelinsky, M., et al. (2020). IL-11 and soluble VCAM-1 are important components of Hypoxia Conditioned Media and crucial for Mesenchymal Stromal Cells attraction. *Stem Cell Res, 45*, 101814.
53. Dicarlo, M., Bianchi, N., Ferretti, C., et al. (2016). Evidence Supporting a Paracrine Effect of IGF-1/VEGF on Human Mesenchymal Stromal Cell Commitment. *Cells, Tissues, Organs, 201*(5), 333–341.
54. Takafuji, Y., Hori, M., Mizuno, T., et al. (2019). Humoral factors secreted from adipose tissue-derived mesenchymal stem cells ameliorate atherosclerosis in Ldlr(-/-) mice [in English]. *Cardiovascular Research, 115*(6), 1041–1051.
55. Min, J. K., Lee, Y. M., Kim, J. H., et al. (2005). Hepatocyte growth factor suppresses vascular endothelial growth factor-induced expression of endothelial ICAM-1 and VCAM-1 by inhibiting the nuclear factor-kappaB pathway. *Circulation Research, 96*(3), 300–307.
56. Huang, J. W., Pong, U. K., Yang, F. Y., et al. (2022). Human pluripotent stem cell-derived ectomesenchymal stromal cells promote more robust functional recovery than umbilical cord-derived mesenchymal stromal cells after hypoxic-ischaemic brain damage [in English]. *Theranostics, 12*(1), 143–166.
57. Gascon, S., Jann, J., Langlois-Blais, C., et al. (2021). Peptides Derived from Growth Factors to Treat Alzheimer's Disease. *International Journal of Molecular Sciences*, *22*(11).
58. Carne, N. A., Bell, S., Brown, A. P., et al. (2019). Reductive Stress Selectively Disrupts Collagen Homeostasis and Modifies Growth Factor-independent Signaling Through the MAPK/Akt Pathway in Human Dermal Fibroblasts [in English]. *Molecular and Cellular Proteomics, 18*(6), 1123–1137.
59. Park, S. R., Kim, J. W., Jun, H. S., et al. (2018). Stem Cell Secretome and Its Effect on Cellular Mechanisms Relevant to Wound Healing. *Molecular Therapy, 26*(2), 606–617.

60. de Araujo, R., Lobo, M., Trindade, K., et al. (2019). Fibroblast Growth Factors: A Controlling Mechanism of Skin Aging. *Skin Pharmacol Physiol, 32*(5), 275–282.
61. Yu, Y., Shen, Y., Zhang, S., et al. (2022). Suppression of cutibacterium acnes-mediated inflammatory reactions by fibroblast growth factor 21 in skin. *International Journal of Molecular Sciences*, *23*(7).
62. Yang, J., Kim, W. J., Jun, H. O., et al. (2015). Hypoxia-induced fibroblast growth factor 11 stimulates capillary-like endothelial tube formation [in English]. *Oncology Reports, 34*(5), 2745–2751.
63. Jeon, S., Kim, N. H., Kim, J. Y., et al. (2009). Stem cell factor induces ERM proteins phosphorylation through PI3K activation to mediate melanocyte proliferation and migration [in English]. *Pigm Cell Melanoma R, 22*(1), 77–85.
64. Tochio, T., Tanaka, H., & Nakata, S. (2013). Glucose transporter member 1 is involved in UVB-induced epidermal hyperplasia by enhancing proliferation in epidermal keratinocytes [in English]. *International Journal of Dermatology, 52*(3), 300–308.
65. Jere, S. W., Houreld, N. N., & Abrahamse, H. (2018). Photobiomodulation at 660nm stimulates proliferation and migration of diabetic wounded cells via the expression of epidermal growth factor and the JAK/STAT pathway. *Journal of Photochemistry and Photobiology B: Biology, 179*, 74–83.
66. Kwon, Y. W., Kwon, K. S., Moon, H. E., et al. (2004). Insulin-like growth factor-II regulates the expression of vascular endothelial growth factor by the human keratinocyte cell line HaCaT [in English]. *Journal of Investigative Dermatology, 123*(1), 152–158.
67. Jo, H., Brito, S., Kwak, B. M., et al. (2021). Applications of Mesenchymal Stem Cells in Skin Regeneration and Rejuvenation. *International Journal of Molecular Sciences*, *22*(5).
68. Spees, J. L., Lee, R. H., & Gregory, C. A. (2016). Mechanisms of mesenchymal stem/stromal cell function. *Stem Cell Research & Therapy, 7*(1), 125.
69. Rani, S., Ryan, A. E., Griffin, M. D., et al. (2015). Mesenchymal Stem Cell-derived Extracellular Vesicles: Toward Cell-free Therapeutic Applications. *Molecular Therapy, 23*(5), 812–823.
70. Mazini, L., Rochette, L., Admou, B., et al. (2020). Hopes and Limits of Adipose-Derived Stem Cells (ADSCs) and Mesenchymal Stem Cells (MSCs) in Wound Healing. *International Journal of Molecular Sciences, 21*(4)
71. Li, J.-Y., Ren, K.-K., Zhang, W.-J., et al. (2019). Human amniotic mesenchymal stem cells and their paracrine factors promote wound healing by inhibiting heat stress-induced skin cell apoptosis and enhancing their proliferation through activating PI3K/AKT signaling pathway [in eng]. *Stem Cell Research & Therapy, 10*(1), 247.
72. Zheng, X., Ding, Z., Cheng, W., et al. (2020). Microskin-Inspired Injectable MSC-Laden Hydrogels for Scarless Wound Healing with Hair Follicles. *Advanced Healthcare Materials, 9*(10), e2000041.
73. Birch-Machin, M. A., & Bowman, A. (2016). Oxidative stress and ageing [in eng]. *British Journal of Dermatology, 175*(Suppl 2), 26–29.
74. Dissemond, J., Schneider, L. A., Brenneisen, P., et al. (2003). Protective and determining factors for the overall lipid peroxidation in ultraviolet al-irradiated fibroblasts: In vitro and in vivo investigations [in eng]. *British Journal of Dermatology, 149*(2), 341–349.
75. Fischer, T. W., Kleszczyński, K., Hardkop, L. H., et al. (2013). Melatonin enhances antioxidative enzyme gene expression (CAT, GPx, SOD), prevents their UVR-induced depletion, and protects against the formation of DNA damage (8-hydroxy-2'-deoxyguanosine) in ex vivo human skin [in eng]. *Journal of Pineal Research, 54*(3), 303–312.
76. Banks, C. J., & Andersen, J. L. (2019). Mechanisms of SOD1 regulation by post-translational modifications. *Redox Biology, 26*, 101270.
77. Eleutherio, E. C. A., Silva Magalhães, R. S., de Araújo, B. A., et al. (2021). SOD1, more than just an antioxidant [in eng]. *Archives of Biochemistry and Biophysics, 697*, 108701.
78 Hernandez-Segura, A., de Jong, T. V., Melov, S., et al. (2017). Unmasking Transcriptional Heterogeneity in Senescent Cells. *Current Biology, 27*(17), 2652-2660.e2654.
79 Pittayapruek, P., Meephansan, J., Prapapan, O., et al. (2016). Role of Matrix Metalloproteinases in Photoaging and Photocarcinogenesis. *International Journal of Molecular Sciences, 17*(6)
80. Sachdev, U., & Lotze, M. T. (2017). Perpetual change: Autophagy, the endothelium, and response to vascular injury. *Journal of Leukocyte Biology, 102*(2), 221–235.
81. Cardoso, A. L., Fernandes, A., Aguilar-Pimentel, J. A., et al. (2018). Towards frailty biomarkers: Candidates from genes and pathways regulated in aging and age-related diseases. *Ageing Research Reviews, 47*, 214–277.
82. Rittie, L., & Fisher, G. J. (2015). Natural and sun-induced aging of human skin. *Cold Spring Harbor Perspectives in Medicine, 5*(1), a015370.
83. Oishi, Y., Fu, Z. W., Ohnuki, Y., et al. (2002). Molecular basis of the alteration in skin collagen metabolism in response to in vivo dexamethasone treatment: Effects on the synthesis of collagen type I and III, collagenase, and tissue inhibitors of metalloproteinases. *British Journal of Dermatology, 147*(5), 859–868.
84. Komi, D. E. A., Khomtchouk, K., & Santa Maria, P. L. (2020). A Review of the Contribution of Mast Cells in Wound Healing: Involved Molecular and Cellular Mechanisms. *Clinical Reviews in Allergy and Immunology, 58*(3), 298–312.
85. Green, D. R., Galluzzi, L., & Kroemer, G. (2011). Mitochondria and the autophagy-inflammation-cell death axis in organismal aging. *Science, 333*(6046), 1109–1112.
86. Ravikumar, B., Sarkar, S., Davies, J. E., et al. (2010). Regulation of mammalian autophagy in physiology and pathophysiology. *Physiological Reviews, 90*(4), 1383–1435.
87. Zhang, X., Cheng, X., Yu, L., et al. (2016). MCOLN1 is a ROS sensor in lysosomes that regulates autophagy [in eng]. *Nature Communications, 7*, 12109.
88. Rubinsztein, D. C., Mariño, G., & Kroemer, G. (2011). Autophagy and aging [in eng]. *Cell, 146*(5), 682–695.
89. Baeken, M. W., Weckmann, K., Diefenthäler, P., et al. (2020). Novel Insights into the Cellular Localization and Regulation of the Autophagosomal Proteins LC3A, LC3B and LC3C [in eng]. *Cells, 9*(10)
90. Huang, R., Xu, Y., Wan, W., et al. (2015). Deacetylation of nuclear LC3 drives autophagy initiation under starvation. *Molecular Cell, 57*(3), 456–466.
91. Kang, C., Xu, Q., Martin, T. D., et al. (2015). The DNA damage response induces inflammation and senescence by inhibiting autophagy of GATA4. *Science, 349*(6255), aaa5612.
92. Young, A. R., Narita, M., Ferreira, M., et al. (2009). Autophagy mediates the mitotic senescence transition. *Genes & Development, 23*(7), 798–803.
93. Cavinato, M., Koziel, R., Romani, N., et al. (2017). UVB-Induced Senescence of Human Dermal Fibroblasts Involves Impairment of Proteasome and Enhanced Autophagic Activity. *Journals of Gerontology. Series A, Biological Sciences and Medical Sciences, 72*(5), 632–639.
94. Demirovic, D., Nizard, C., & Rattan, S. I. S. (2015). Basal level of autophagy is increased in aging human skin fibroblasts in vitro, but not in old skin [in eng]. *PLoS ONE, 10*(5), e0126546.